sustainability

MDPI

Article

Fatigue Life Prediction for Semi-Closed Noise Barrier of High-Speed Railway under Wind Load

Xiaoping Wu [1,2], Ye Zhu [1,*], Lingxiao Xian [1] and Yingkai Huang [1]

[1] Department of Civil Engineering, Central South University, Changsha 410075, China; xpwu@csu.edu.cn (X.W.); 184812196@csu.edu.cn (L.X.); 184812201@csu.edu.cn (Y.H.)
[2] Centre for Transportation Studies, University College London, London WC1E6BT, UK
* Correspondence: csuzhuye@csu.edu.cn

Abstract: The fatigue state of the semi-closed noise barrier directly affects driving safety, and replacement after damage leads to train delays and increased operating costs. It is more eco-friendly and sustainable to predict the fatigue life of noise barriers to reinforce the structure in time. However, previous life prediction methods provide a limited reference in the design stage. In this study, a novel fatigue life prediction method for noise barriers was proposed. The computational fluid dynamics and finite element model of the semi-closed noise barrier were established and subjected to simulated natural wind and train aerodynamic impulse wind loads to calculate the stress time-history on the noise barrier. Based on the rain flow counting method and Miner linear cumulative fatigue damage theory, the fatigue life of noise barriers in three Chinese cities was predicted. The results show that the fatigue life of the noise barrier is closely related to the wind conditions and train operation modes. Targeted reinforcement for noise barriers in different fatigue states can save materials and reduce maintenance workload. Moreover, the influence of wind load on the noise barrier was summarized, and engineering suggestions on prolonging the fatigue life of noise barriers were put forward.

Keywords: semi-closed noise barrier; wind load; fatigue life prediction; finite element method; Miner linear cumulative fatigue damage theory; sustainability

Citation: Wu, X.; Zhu, Y.; Xian, L.; Huang, Y. Fatigue Life Prediction for Semi-Closed Noise Barrier of High-Speed Railway under Wind Load. *Sustainability* **2021**, *13*, 2096. https://doi.org/10.3390/su13042096

Academic Editor: Marinella Silvana Giunta

Received: 18 January 2021
Accepted: 11 February 2021
Published: 16 February 2021

1. Introduction

The rapid development of high-speed railways (HSRs) drives the economy, while the increasing train speed increases the noise pollution associated with train operations [1]. Studies have shown that when the train speed exceeds 300km/h, the aerodynamic noise surpasses the wheel-rail noise which is the primary noise source [2]. Thus, the noise barrier has become an important measure to reduce noise along the railway. The most widely used type is the vertical noise barrier [3–5]. Limited by its height and shape, the common vertical noise barrier has insufficient noise reduction effects in high-rise residential areas and ecological protection areas, consequently, it cannot sufficiently meet noise reduction requirements in some specific cases. Therefore, the semi-closed noise barrier, with better noise reduction effects, is gradually gaining acceptance for application in practice [6,7].

Until now, the research on semi-closed noise barriers has mainly focused on the noise reduction effect, aerodynamic impulse pressure distribution, and dynamic response. In experimental research, Denis Duhamel, Zhang Xun, etc. studied the noise transmission path and the acoustic characteristics of the semi-closed noise barrier through the field monitoring of HSR, and verified the noise reduction effect of the semi-closed noise barrier, it was found out that the resonance effect reduces the noise reduction effect of the semi-closed noise barrier [8–10]; Munemasa Tokunaga studied the dynamic response characteristics of the inward-folded noise barrier of HSR through field measurement [11]. Using numerical techniques, Lu Ming and Zhou Qiang established the noise prediction model of the semi-closed noise barrier to study the noise reduction effect and application scope of semi-closed and fully closed noise barriers. The numerical results were verified

by their experiments [12,13]; He Jiajun established a fully closed noise barrier model to study the characteristics of aerodynamic impulse pressure generated when trains enter the noise barrier area under different working conditions [14]. Luo Yunke, Jing Zheng established the computational fluid dynamics model and finite element model to calculate the aerodynamic impulse wind pressure and dynamic response of the semi-closed noise barrier. Compared with the vertical noise barrier, the semi-closed noise barrier is higher and more airtight, so the natural wind and train aerodynamic impulse wind loads have a greater influence on it [15,16].

Research on noise reduction and vibration performance of noise barriers has been fully explored and this has provided theoretical support for the design stage of noise barriers. However, in practical engineering, the noise barrier along the German HSR has encountered problems such as panel breakage and loosening of the connecting bolts between the column and the base. Hence, the noise barriers were removed to ensure driving safety, which caused much economic loss [17]. Therefore, to highlight the concept of eco-friendly and sustainable development, the fatigue performance of noise barriers should be of great concern. It is of significant engineering value to predict the fatigue life of noise barriers, and then strengthen the noise barriers with potential damage in time and replace the components pertinently to prolong the service time.

For the sustainable development of railway transportation, predicting the service life of railway facilities and then evaluating the maintenance plan can improve the economic competitiveness of railways. P. Di Mascio proposed a method to access the railway structural distress produced by fatigue and rutting of a railway and to evaluate maintenance work costs, which can be used to define maintenance plans [18]. However, there are few studies on the life prediction of noise barriers. Thomas Keller, Sun Yuan, and Lachinger studied the load-bearing limit and fatigue performance of noise barrier components under train aerodynamic impulse wind through field experiments, and propounded suggestions for calculating the dynamic response and fatigue damage of noise barriers [19–21]. A lifespan prediction technique for digital twin-based noise barrier tunnels was proposed by J. Kim, but this method can only be used in the production stage of noise barriers and cannot be applied in the case of noise barriers under operation, owing to budgetary restrictions [22]. In the research above, the fatigue life of the noise barrier was predicted by the physical movement of the structural components in practice, which cannot be predicted before installation. Moreover, these studies were carried out in some specific cases and working conditions, so the conclusions are not generalizable. Therefore, in the design and planning stage, the fatigue life of noise barriers can only be predicted by numerical simulation.

In this study, a universal fatigue life prediction method for the semi-closed noise barrier was proposed. The design concepts and calculation process of this method can be justified from the life prediction methods of other structures [23,24]. This research was carried out by the technical route shown in Figure 1.

According to the technical route shown in Figure 1, the remainder of this paper is organized as follows. Firstly, the computational fluid dynamics (CFD) and finite element method (FEM) models of the semi-closed noise barrier in HSR were established. Sections 2 and 3 present the simulation process and verification of natural wind and train aerodynamic impulse wind, respectively. In Section 4, the dynamic response of noise barriers under wind load was studied using the FEM model. Based on the rain flow counting (RFC) method and linear cumulative fatigue damage (LCFD) theory, the fatigue life of noise barriers in three Chinese cities under different operation conditions was predicted. Section 5 presents the advantages of this fatigue life prediction method. Furthermore, engineering suggestions for prolonging the fatigue life of noise barriers were put forward. Finally, Section 6 summarizes the conclusions of this study. The findings of this study can serve as a good reference in the design and maintenance stage of the semi-closed noise barrier, thereby enhancing sustainability.

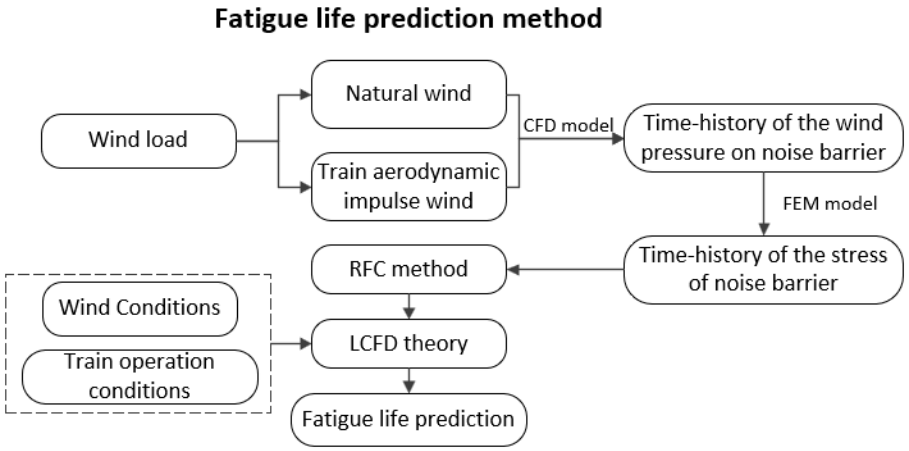

Figure 1. The technical route of this study.

2. Natural Wind Load Calculation

2.1. Natural Wind Simulation

The downwind time-history of wind contains two parts: the average wind and the pulsating wind. In this study, the pulsating wind time-history was simulated by the harmonic superposition method [25], and the Kaimal wind speed spectrum [26] was selected according to the Chinese standard pulsating wind speed power spectrum [27]. The pulsating wind $S_v(n)$ is presented in Equation (1) below.

$$S_v(n) = 200u_0^2 \frac{x^2}{n(1+50x)^{5/3}} \quad (1)$$

where u_0 is the friction speed (m/s^2), $x = nz/v(z)$, n is the frequency (Hz), z is the height (m),$v(z)$ is the average wind speed at height z (m/s^2).

The average wind speed was determined by the commonly used exponential wind profile formula, presented in Equation (2) below.

$$v(z) = v_0\left(\frac{z}{z_0}\right)^{\alpha} \quad (2)$$

where z_0 is the standard height (m), generally 10 m, v_0 is the average wind speed at the standard height (m/s^2), α is the index coefficient related to the terrain or terrain roughness, the greater the roughness of the ground, the greater the α.

The spatial correlation of simulation points was determined according to the empirical formula proposed by Davenport [28], as presented in Equation (3) below.

$$coh(f, \Delta) = \exp\left(-c\frac{fd}{\overline{v}(z)}\right) \quad (3)$$

where c is the space-related attenuation coefficient, f is the pulsating wind frequency (Hz), d is the distance between spatial points (m).

Based on the theory of harmonic synthesis, the random wind speed synthesis program was compiled by considering the fluctuating wind speed, average wind speed, and other parameters. When the average wind speed at the standard height of 15 m above the ground was 15 m/s, the random wind speed time history was simulated and shown in Figure 2a below. To verify the reliability of the simulated random wind speed, the power spectrum of the simulated fluctuating wind was calculated and compared with the Kaimal wind speed spectrum in the specification as shown in Figure 2b below. It can be seen from Figure 2b that the simulated spectrum is consistent with the target spectrum, which meets the requirements of fluctuating wind field characteristics.

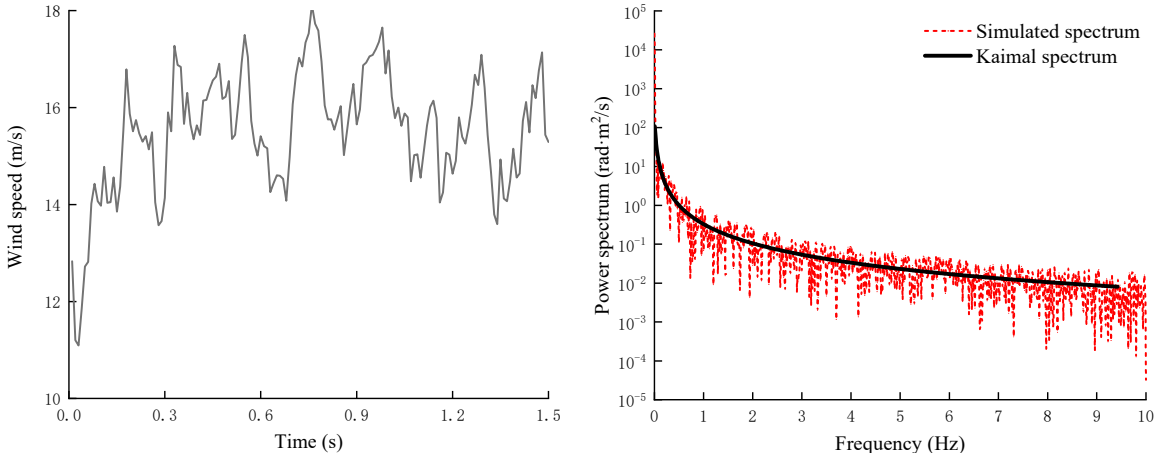

Figure 2. The random natural wind simulation and its verification. (**a**) time-history of the simulated natural wind speed; (**b**) comparison between the simulated and target power spectrum.

2.2. Natural Wind Pressure on the Noise Barrier

When the natural wind speed is greater than 20 m/s, high-speed trains need to run within a speed limit [29]. Therefore, the 10-span semi-closed noise barrier was taken as the research object, with a height and length of 8.15 m and 20 m respectively. The natural wind speeds at a height of 15 m above the ground under the wind speed of 1~8 level were simulated under the simulation time was 1.5 s. In order to obtain the natural wind pressure on the noise barrier under the varying wind speed, Equation (4) was adopted for conversion [30].

$$w = \rho \times v^2 \tag{4}$$

where w is the wind pressure (Pa); ρ is the air density, generally 1.293 kg/m^3; v is the wind speed (m/s^2).

The time-histories of the pressure on the 1st to 10th span panels of noise barriers under the third-level wind speed is shown in Figure 3, while the maximum pressure of noise barrier panels under all levels of wind speed and the annual statistics of wind speed in three Chinese cities is shown in Table 1. It can be seen from Table 1 that the wind pressure on the semi-closed noise barrier increases with the increase of natural wind speed, and the growth rate is increasing.

Table 1. Maximum wind pressure on noise barrier under varying wind speeds and the annual wind speed statistics in three Chinese cities.

Statistical Indicators	Wind Speed Level							
	One	Two	Three	Four	Five	Six	Seven	Eight
Average wind speed (m/s)	1.5	3.3	5.4	7.9	10.7	13.8	17.1	20.7
Maximum wind pressure (Pa)	4.7	26.3	72.9	187.0	372.5	659.2	1056.1	1590.9
Annual duration in Beijing (days)	107	170	58	21	6	2	1	0
Annual duration in Shanghai (days)	230	81	43	8	2	0.5	0.25	0.25
Annual duration in Shenzhen (days)	109.5	117.0	68.0	67.0	2.0	1.0	0.5	0.5

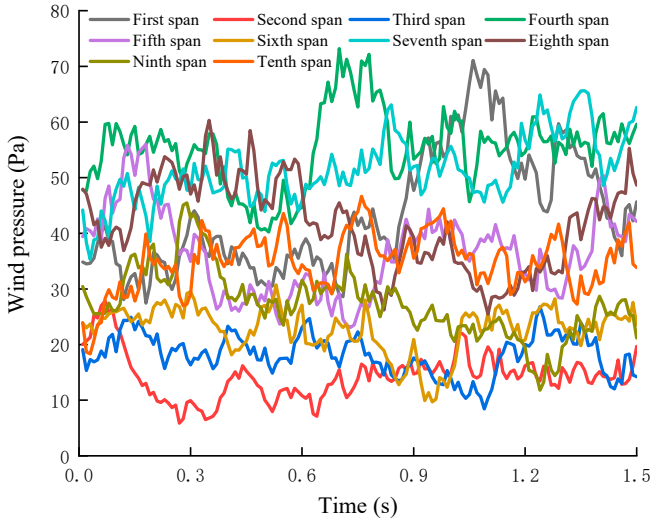

Figure 3. Pressure on each span of the noise barrier under the third-level wind speed.

3. Aerodynamic Impulse Wind Load Calculation

3.1. Train-Noise Barrier External Flow Field Model

In this study, the commercial software FLUENT was used to establish the CFD model and calculate the wind pressure on the noise barrier. The high-speed train CRH380A simplified into a three-group train model composed of a head train, middle train, and tail train was taken as the research object [31]. The length, height, and width of the train model were 78 m, 3.6 m, and 3.4 m, respectively. Grid encryption was carried out on key parts such as the front and rear of the train and the surface of the noise barrier. The total number of grids was about 6 million. The semi-closed noise barrier was established, with the height and length of 8.15 m and 300 m respectively. The railway line spacing was 5 m. The calculation domain of the external flow field was 400 × 140 × 60 m and the slip grid area was 650 × 5 × 5 m. The solid boundaries such as the train surface, the track-bed top surface, and the noise barrier surface were all set as the non-slip wall boundary. The front and back of the calculation domain were set as the pressure outlet boundary, and the contact surface between the moving area and the static area was set as the interface. When the high-speed train passes through a noise barrier, the train head constantly compresses the surrounding air, thereby, forming a three-dimensional, viscous, and compressible unsteady turbulent field. In the calculation, the RNG k-ε two-equation model was selected, and the sliding-grid method was used to simulate the process of the high-speed train entering and leaving the semi-closed noise barrier. The working conditions included different noise barrier layout forms (single-sided semi-closed noise barrier, double-sided semi-closed noise barrier), different train speeds (350 km/h, 400 km/h), and different train operation modes (single train running, two trains meeting). The specific layouts of high-speed trains and noise barrier conditions are shown in Figure 4.

In the numerical simulation, different methods and parameters may lead to different calculation results. Deutsche Bahn has tested the train aerodynamic impulse pressure on the vertical noise barrier through field tests [32]. Therefore, the railway parameters of that field test were used to establish a noise barrier model for calculation. The simulation results were compared with the test results of the German railway to verify the effectiveness of the numerical simulation method and parameters adopted in this study. Figure 5 shows the comparison between the time history of simulated aerodynamic impulse pressure and that of measured pressure when the train speed is 300 km/h.

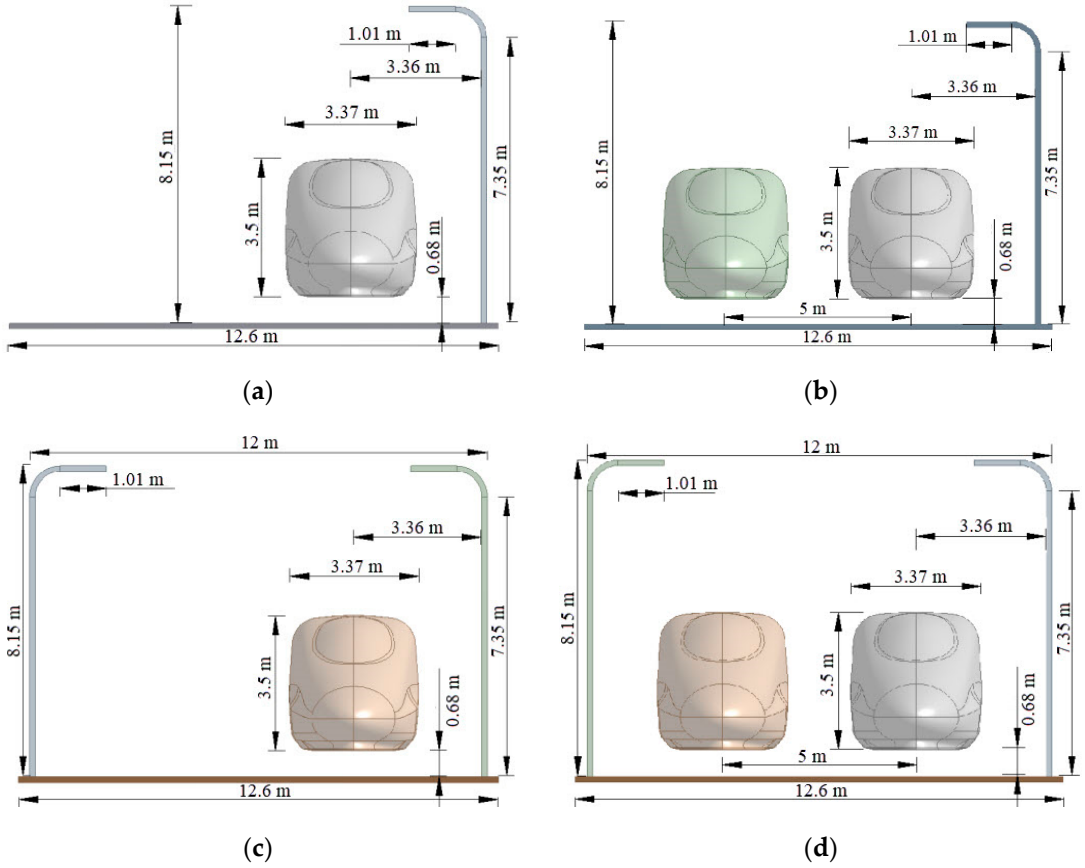

Figure 4. Schematic type of the train operation modes and the noise barrier layouts. (**a**) single-track railway with single-sided noise barrier; (**b**) double-track railway with single-sided noise barrier; (**c**) single-track railway with double-sided noise barrier; (**d**) double-track railway with double-sided noise barrier.

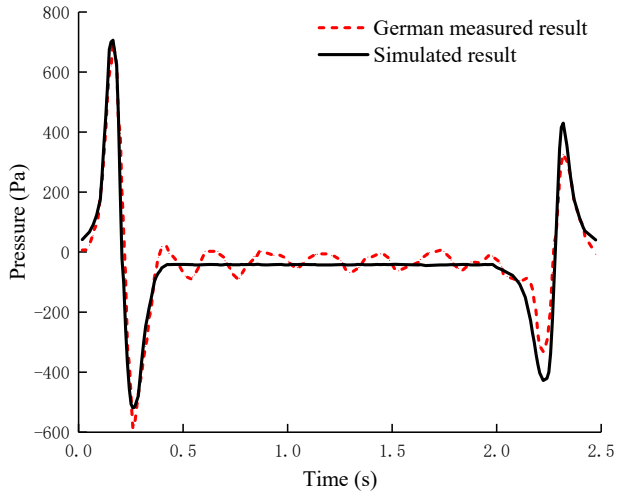

Figure 5. Comparison between the simulated and measured aerodynamic impulse pressure.

It can be seen from Figure 5 that the simulated aerodynamic impulse pressure is consistent with the measured pressure. When the train enters the noise barrier area, the aerodynamic load on the noise barrier surface presents a positive pressure field first and then a negative pressure field called the "head wave". When the train leaves the noise barrier area, the aerodynamic load on the noise barrier surface presents a negative pressure field first and then a positive pressure field, called the "tail wave". The maximum

positive and negative pressures of the "head wave" are greater than that of the "tail wave". Due to the proper simplification of the train model, the simulated aerodynamic impulse pressure is slightly different from the measured wind pressure. When the train body passes through the noise barrier, the measured pressure curve of the noise barrier fluctuates, while the simulated curve remains smooth. This is because the train wheels, couplers, and pantographs were omitted in the simplified model with less train formation. The maximum simulated fluctuating wind pressure of the noise barrier is 1.1% larger than the measured value when the train head and tail pass by, so it is safer to check the fatigue performance by using the simulated train aerodynamic impulse pressure.

From the foregoing, it can be deduced that the simulation method adopted in this study can accurately simulate the aerodynamic impulse pressure on the noise barrier when the high-speed train passes through it.

3.2. Analysis of Flow Field Calculation Results

The semi-closed noise barrier's dynamic performance under different working conditions was simulated. Figure 6a shows the aerodynamic impulse pressure cloud chart of the noise barrier along the track axis at a certain time when the train passes at 350 km/h. It can be seen from Figure 6a that the noise barrier sections corresponding to the train head and tail are subjected to large aerodynamic impulse pressure. Therefore, these four cross sections, corresponding to the train nose tip, the train head, the train tail, and the train tail tip, respectively, were selected to show the aerodynamic impulse pressure cloud chart of the external flow field, as shown in Figure 6b–e. They correspond to the first to fourth cross sections marked in Figure 6a.

As shown in Figure 6, the aerodynamic impulse pressure around the train is the largest and decreases in a diffused way, so the corresponding position of the noise barrier panel is in a "pressure target" shape. The bottom flow field is hindered by the train, noise barrier, and track-bed, which makes the air flow space small and the air circulation speed slow. Therefore, the pressure center of the noise barrier appears at the bottom. Along the height direction of the noise barrier, the flow field space becomes more and more open and the effect of the train aerodynamic impulse wind weakens, thus, the pressure on the noise barrier decreases.

Moreover, the time-histories of the aerodynamic impulse pressure on the noise barrier panels near the train side are shown in Figure 7. Table 2 shows the statistics of peak aerodynamic impulse pressure on the noise barrier under different working conditions.

Table 2. Peak aerodynamic impulse pressure on the noise barrier under different working conditions (Pa).

Train Operation Mode	Noise Barrier Layout and Train Speed			
	Single-Sided Noise Barrier		Double-Sided Noise Barrier	
	350 km/h	400 km/h	350 km/h	400 km/h
One train running	863.05	1128.97	876.30	1143.64
Two trains meeting	1071.67	1378.73	1137.78	1472.20

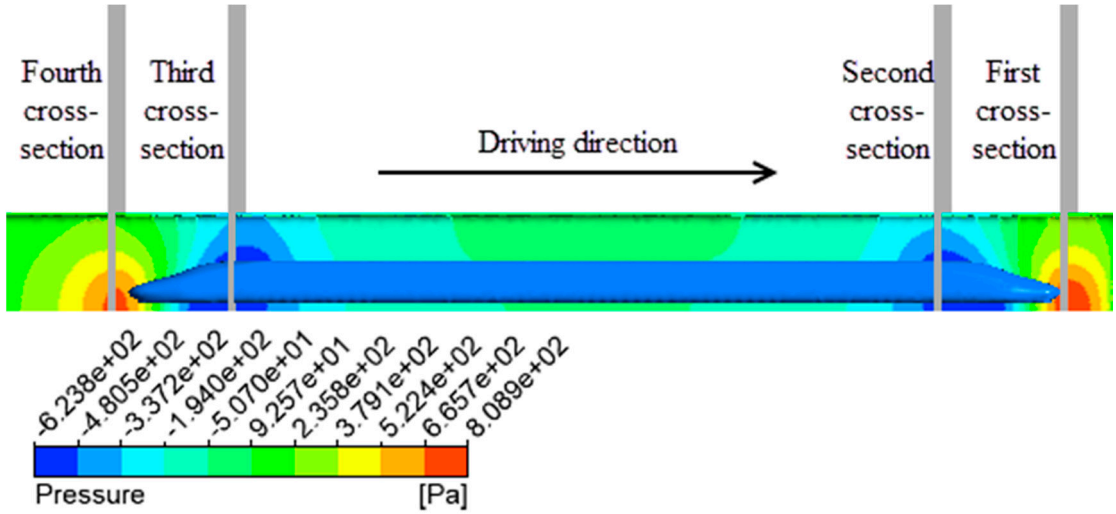

(**a**)

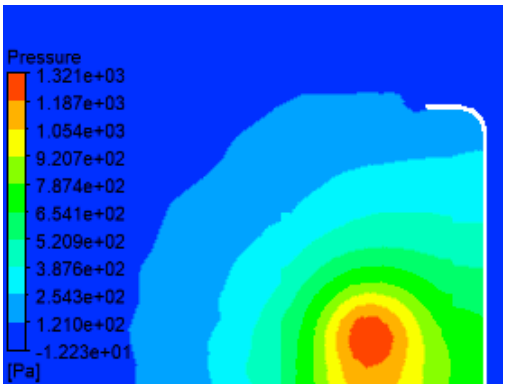

(**b**)

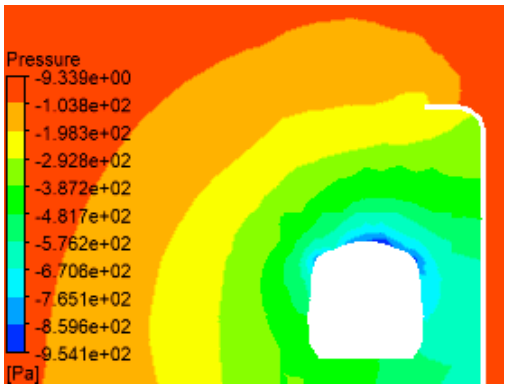

(**c**)

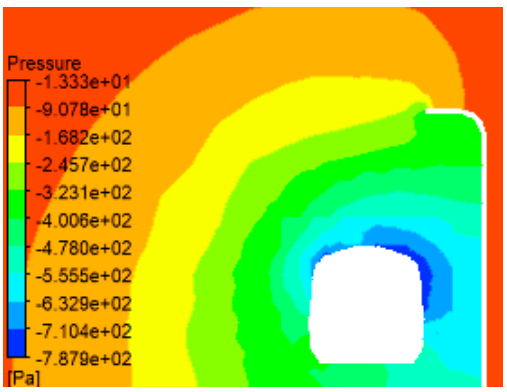

(**d**)

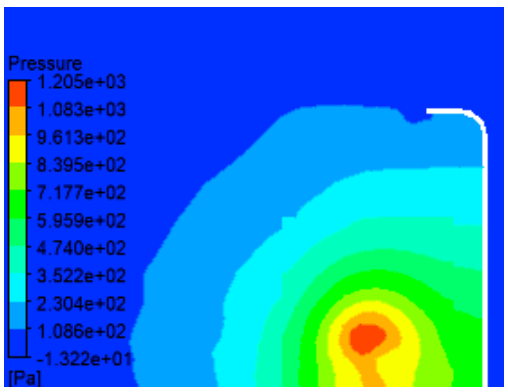

(**e**)

Figure 6. The aerodynamic impulse pressure cloud chart of the noise barrier and the external flow field. (**a**) the cloud chart of the noise barrier along the track axis; (**b**) the first cross-section; (**c**) the second cross-section; (**d**) the third cross-section; (**e**) the fourth cross-section.

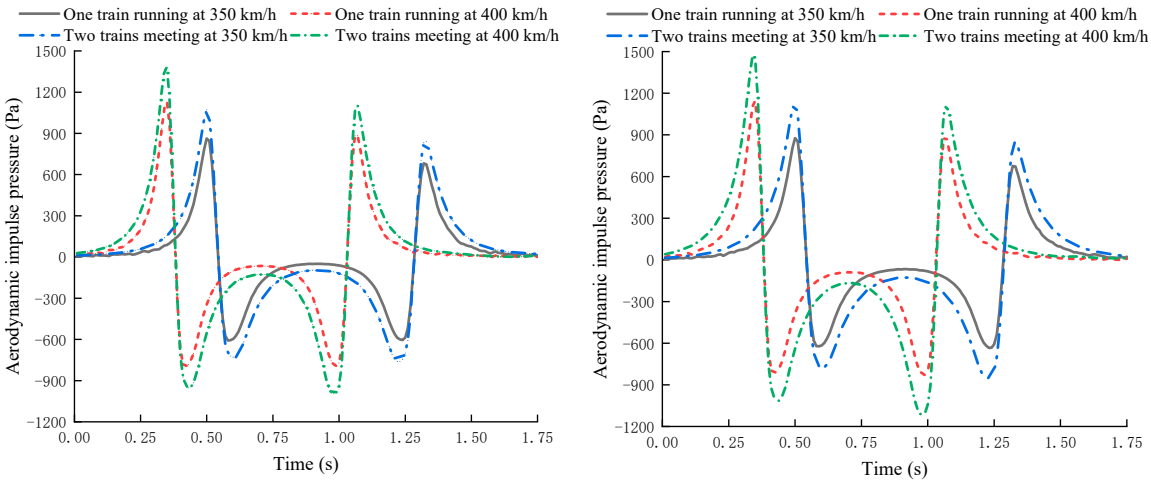

Figure 7. Time-histories of aerodynamic impulse pressure on the semi-closed noise barrier panels under different working conditions. (**a**) single-sided noise barrier; (**b**) double-sided noise barrier.

It can be seen from Figure 7 and Table 2 that the trends of the aerodynamic impulse pressure time-histories of the noise barrier under different working conditions are consistent. Also, the "head wave" and "tail wave" appear in the aerodynamic impulse pressure time-history of the semi-closed noise barrier, which is consistent with the pressure on the vertical noise barrier. As the train speed increases, the aerodynamic impulse pressure on the semi-closed noise barrier increases. When the train speed increases from 350 km/h to 400 km/h, the maximum aerodynamic impulse pressure increases by more than 28% under different working conditions. Different noise barrier layouts also influence the aerodynamic impulse pressure on the noise barrier. Since the structure of the double-sided semi-closed noise barrier is more airtight, the maximum wind pressure on the double-sided semi-closed noise barrier under all working conditions is higher than that on the single-sided semi-closed noise barrier. The maximum aerodynamic impulse pressure difference between the two layouts is about 1.4% under a single train running, and 6.3% under two trains meeting. Moreover, different train operation modes have a great impact on the aerodynamic impulse pressure on the noise barrier. The aerodynamic impulse pressure caused by two trains meeting is higher than that caused by a single train running. When the train passes through the single-sided semi-closed noise barrier at 350 km/h and 400 km/h, the maximum pressure difference between the two modes is 24.2% and 22.1%, respectively. When the train passes through the double-sided noise barrier, the maximum wind pressure difference between the two modes is 29.8% and 28.7%, respectively. Among all working conditions, the maximum aerodynamic impulse pressure 1472.20 Pa is obtained when two trains pass each other at 400km/h through the double-sided semi-closed noise barrier.

It is indicated that the aerodynamic impulse pressure on the noise barrier is a time-varying load and is affected by many factors. Loading the maximum or average wind pressure to the noise barrier cannot reflect the actual pressure on the noise barrier. Therefore, in this study, the aerodynamic impulse pressure time-histories on the noise barrier were loaded onto the structure for the fatigue calculation of the semi-closed noise barrier.

4. Fatigue Performance Analysis

4.1. Fatigue Damage Theory

In the structural fatigue analysis, the Miner linear fatigue cumulative damage theory [33] was used to estimate the fatigue life of the noise barrier. The calculation for

structural damage D is shown in Equation (5). When the total damage D reaches 1 under k times stress amplitudes σ_i, fatigue failure occurs in the structure.

$$D = \sum_{i=1}^{k} \frac{n_i}{N_i} \tag{5}$$

where n_i is the cycles of the structure under the stress amplitude σ_i (times), N_i is the total number of cycles damage occurs (times), $N_i = (\Delta\sigma_i)^{-\beta/c}$, $\Delta\sigma_i$ is the fatigue allowable stress amplitude, c and β are the correlation coefficients between components and connections [34].

The pulse force on the noise barrier is an alternating aerodynamic load. Based on the stress time-history obtained above, the rain flow counting method was used to obtain the stress spectrum of natural wind and train aerodynamic impulse load. Furthermore, the cycles n_i under each stress amplitude σ_i were calculated. When the natural wind continuously loads on the noise barrier, Equation (6) can be derived to compute the fatigue life of the noise barrier y_1.

$$y_1 = \frac{(\Delta\sigma_i)^{-\beta}}{c \cdot 57600 \cdot d \cdot n_i} \tag{6}$$

where y_1 is the fatigue life of noise barrier under the natural wind (years), d is the time of occurrence of natural winds at all levels in a year (days).

When the HSR passes through a pairs of trains in one day, Equation (7) can be derived to compute the fatigue life of the noise barrier y_2.

$$y_2 = \frac{(\Delta\sigma_i)^{-\beta}}{c \cdot 365 \cdot a \cdot n_i} \tag{7}$$

where y_2 is the fatigue life of noise barrier under the train aerodynamic impulse wind (years), a is the number of high-speed trains passing through the semi-closed noise barrier in one day (pairs).

According to the fatigue theory above, the fatigue life of a semi-closed noise barrier under natural wind, train aerodynamic impulse wind, and their combined load was predicted.

4.2. Noise Barrier Finite Element Model

Based on the physical model of the semi-closed noise barrier in the HSR, the software ANSYS WORKBENCH was used to establish the FEM model and calculate the stress of the noise barrier. A finite element model of a 10-span semi-closed noise barrier was established with a height and length of 8.15 m and 20 m respectively, as presented in Figure 8. The distance between the columns is 2 m, and 13 aluminum alloy composite sound-absorbing panels with a height of 0.45 m are arranged along the height direction. The length of the panel at the top is 1.01 m. A transparent sound insulation panel with a height of 1 m is set between the fifth and the sixth panel, and one with a radius of 0.8 m is set at the corner. The columns, beams, bottom plates, and stiffening plates are made of Q235 carbon structural steel, and the sound-absorbing panels and the transparent sound insulation panels are made of 5A03 aluminum alloy and polycarbonate, respectively. The material parameters are shown in Table 3.

Table 3. Material parameters used in the noise barrier FEM model.

Materials	Density (kg/m^3)	Elastic Modulus (GPa)	Poisson's Ratio
Q235 steel	7850	200	0.3
5A03 Aluminum alloy	2670	72	0.3
Polycarbonate	1200	2.32	0.4

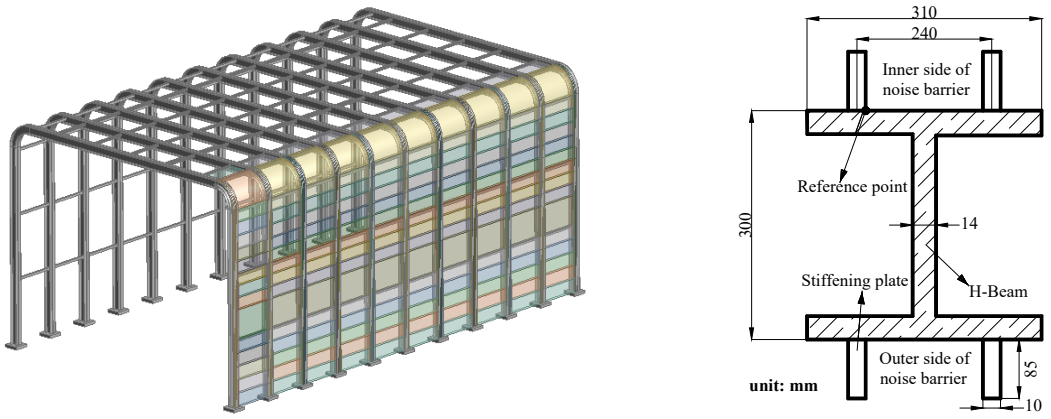

(**a**) (**b**)

Figure 8. The finite element model and reference point of semi-closed noise barrier. (**a**) the finite model of noise barrier; (**b**) the steel column cross-section dimensions and the location of reference point.

Based on the calculation above, the fatigue life of the semi-closed noise barrier near the train side was calculated under different layouts, different train speeds, and different train operation modes. The noise barrier can be regarded as a cantilever beam, and the stress at the bottom of the H-shaped steel column is the largest, so, the joint point between the H-shaped steel and stiffening plate was selected as the reference point.

4.3. Fatigue Performance Analysis of Noise Barrier under Natural Wind Load

The time-histories of varying natural wind levels calculated previously were sequentially loaded onto the noise barrier to calculate the time history of the equivalent stress at the bottom reference point. Figure 9 shows the results obtained. Table 4 shows the peak stress of the semi-closed noise barrier corresponding to each wind level.

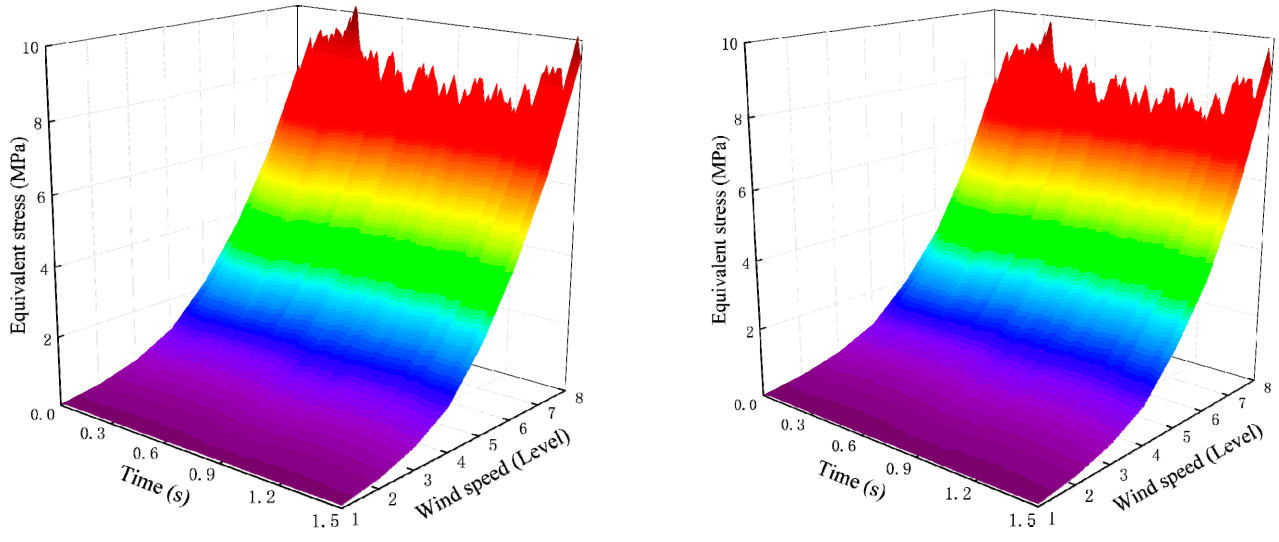

(**a**) (**b**)

Figure 9. Time-history of equivalent stress of the semi-closed noise barrier at various wind speeds. (**a**) single-sided noise barrier; (**b**) double-sided noise barrier.

Table 4. Corresponding maximum stress of semi-closed noise barrier at each wind speed level (MPa).

Noise Barrier Layouts	Wind Speed Level							
	One	Two	Three	Four	Five	Six	Seven	Eight
Single-sided noise barrier	0.10	0.30	0.70	1.41	2.77	4.68	7.10	10.20
Double-sided noise barrier	0.09	0.27	0.62	1.23	2.47	4.13	6.60	9.82

It can be seen from Figure 9 and Table 4 that as the wind speed increases, the equivalent stress of the semi-closed noise barrier increases, and the growth rate continues to increase. The variation trends of the equivalent stress of the single-sided noise barrier are consistent with that of the double-sided noise barrier, however, the maximum equivalent stress of the single-sided noise barrier is slightly larger than that of the double-sided noise barrier. Under the first-level wind speed, the maximum equivalent stress of single-sided and double-sided noise barriers is 0.10 MPa and 0.09 MPa, respectively; under the eight-level wind speed, the maximum equivalent stress of single-sided and double-sided noise barriers is 10.20 MPa and 9.82 MPa, respectively. Different layouts have little influence on the noise barrier under natural wind. Compared with the single-sided semi-closed noise barrier, the double-sided noise barrier has the top frame connection between the two sides, which makes the structure possess better integrity and greater rigidity, so its equivalent stress is slightly smaller than that of the single-sided type.

The time-histories of equivalent stress at the reference points were counted by the rain flow counting method to obtain the stress spectrum corresponding to different working conditions. Through the annual duration of each wind level in different Chinese cities in Table 1, the fatigue life of semi-closed noise barriers under the independent action of natural wind was calculated, as shown in Figure 10.

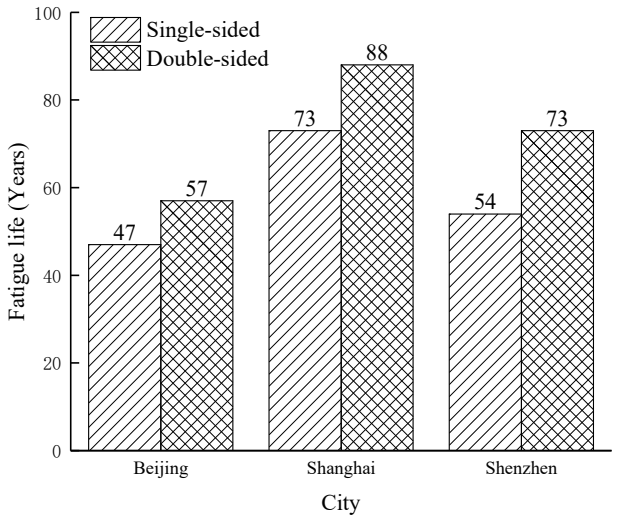

Figure 10. Fatigue life prediction for the semi-closed noise barriers under the natural wind.

As shown in Figure 10, different cities have different wind conditions, so the fatigue life of noise barriers is different. Under natural wind, the fatigue life of the single-sided noise barrier in Beijing, Shanghai, and Shenzhen is 47 years, 73 years, and 54 years, respectively; the fatigue life of the double-sided noise barrier is 57 years, 88 years, and 73 years, respectively. This is because Beijing is located in the North China Plain and Shenzhen is located in the coastal area, so the wind is strong, thus affecting the fatigue life. In addition, when the wind speed exceeds 10 m/s, the natural wind has a great influence on the fatigue life of the noise barrier, so there is a great risk of damage to the noise barrier in strong wind areas.

4.4. Fatigue Performance Analysis of Noise Barrier under Aerodynamic Impulse Wind Load

The calculated aerodynamic impulse pressure time-histories were loaded on the noise barrier structure to obtain the equivalent stress time-history at the reference point of the noise barrier, as shown in Figure 11.

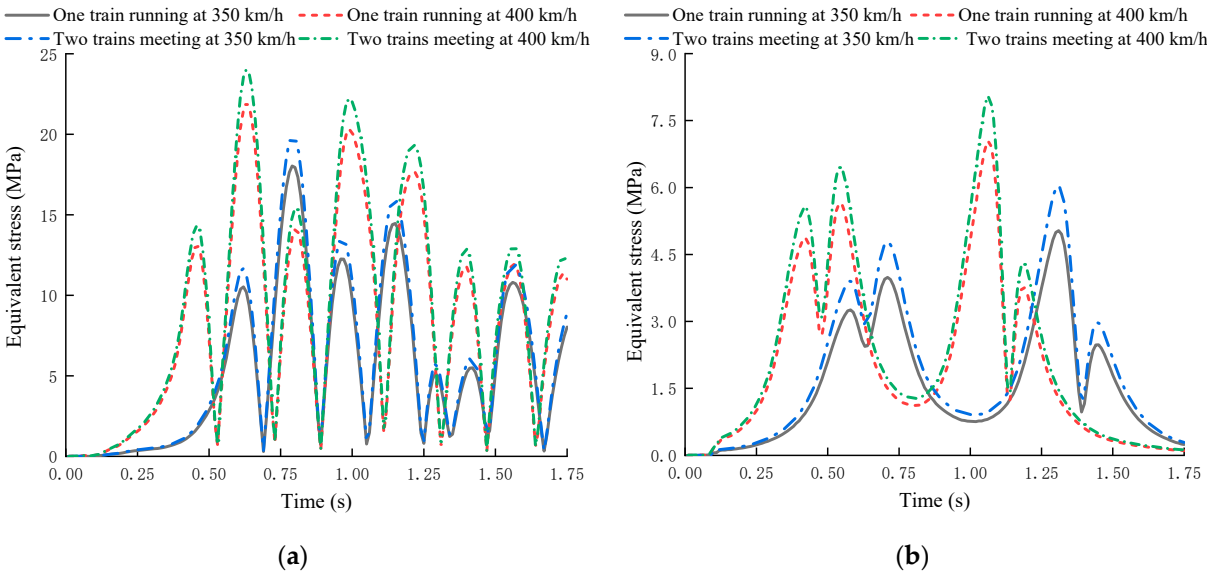

Figure 11. Time-histories of equivalent stress at the reference point of the semi-closed noise barrier under different working conditions. (**a**) single-sided noise barrier; (**b**) double-sided noise barrier.

Similar to the variation trend of the wind pressure, the peak equivalent stress of the noise barrier increases with the increase of the train speed, but the peak stress of the double-sided semi-closed noise barrier is much smaller than that of the single-sided semi-closed noise barrier. Contrary to the fact that the natural wind always acts on the noise barrier with the same wind direction, when the train passes through the noise barrier, the aerodynamic impulse pressure on both sides of the double-sided semi-closed noise barrier appeared to be in opposite directions. Due to the connection of the top frame, the structural deformation of the double-sided noise barrier is small, so the equivalent stress is smaller than that of the single-sided noise barrier. Under the most unfavorable conditions, the maximum stress at the reference point of the single-sided semi-closed noise barrier and the double-sided semi-closed noise barrier is 24.03 MPa and 8.14 MPa, respectively.

Besides, compared with the aerodynamic impulse pressure time-history, the equivalent stress time-history of the single-sided semi-closed noise barrier is "jumping", with frequent peaks and some hysteresis. This is due to the continuity of the noise barrier structure that makes the stress at the reference point have a cumulative effect, and the aerodynamic impulse pressure at the "head wave" and "tail wave" changes sharply. The single-sided semi-closed noise barrier structure is of little symmetry, so, the stress at the reference point of the single-sided noise barrier changes greatly with aerodynamic impulse pressure. With better structural integrity, the stress time-history of the double-sided semi-closed noise barrier is smooth, and the trend is consistent with the wind pressure time-history trend, with more significant stress peaks.

The fatigue life of the noise barrier should be 50 years when passing 210 pairs of trains a day [35]. In the operation of HSR, single-train-running and two-trains-meeting trains alternately appear, and the fatigue life of the noise barrier was calculated according to the trains meeting ratio. The fatigue life of trains passing through the semi-closed noise barrier at different speeds and different train operation modes is shown in Table 5.

Table 5. Fatigue life of noise barrier under train aerodynamic impulse wind load (years).

Trains Meeting Ratio (%)	Noise Barrier Layout and Train Speed			
	Single-Sided Noise Barrier		Double-Sided Noise Barrier	
	350 km/h	400 km/h	350 km/h	400 km/h
0	261.79	90.01	639.03	343.47
20	194.17	79.88	563.97	290.69
50	140.05	69.43	479.46	236.97
80	109.24	61.35	416.67	200.43
100	94.97	55.76	383.14	181.16

It can be seen from Table 5 that the fatigue life of the semi-closed noise barrier can meet the requirement of 50 years under the aerodynamic impulse wind. The fatigue life of the noise barrier decreases with the increase in train speed and the trains meeting ratio. Since the equivalent stress of the double-sided semi-closed noise barrier is small, the fatigue life is more than 100 years, which indicates the fatigue safety performance has redundancy.

4.5. Fatigue Performance Analysis of Noise Barrier under the Combined Load of the Natural Wind and Train Aerodynamic Impulse Wind

In practical engineering, natural wind load and the train pulsating wind load usually act together or alternately on the noise barrier. At the same time, in linear fatigue damage accumulation theory, fatigue damage is independent of the loading sequence of loads, hence, the two can be approximated as the same type of fatigue excitation. Therefore, the fatigue life of the semi-closed noise barrier under different working conditions was calculated by linear superposition of natural wind and aerodynamic impulse wind load, as shown in Table 6.

Table 6. Fatigue life prediction for noise barrier under natural wind and train aerodynamic impulse wind (years).

City	Trains Meeting Ratio (%)	Noise Barrier Layout and Train Speed			
		Single-Sided Noise Barrier		Double-Sided Noise Barrier	
		350 km/h	400 km/h	350 km/h	400 km/h
Beijing	0	39.87	30.90	52.88	49.73
	20	37.88	29.83	52.60	48.51
	50	35.22	28.51	51.54	46.63
	80	32.87	26.74	50.63	44.74
	100	31.17	25.47	50.10	43.72
Shanghai	0	58.72	42.42	77.51	71.12
	20	55.25	40.27	77.28	68.66
	50	49.15	36.56	76.46	65.27
	80	44.96	34.01	73.81	62.20
	100	42.19	32.16	72.38	60.51
Shenzhen	0	44.98	32.89	65.16	60.03
	20	42.46	31.76	64.72	58.39
	50	39.15	30.40	62.73	56.12
	80	36.27	28.74	62.10	53.36
	100	34.18	27.33	61.39	52.30

From Tables 5 and 6, it is indicated that the fatigue life of the semi-closed noise barrier under the combined loads of natural wind and the train aerodynamic impulse wind is greatly reduced compared to that under the train aerodynamic impulse wind independently. Therefore, the influence of natural wind is of great significance for the fatigue life prediction of the semi-closed noise barrier. As shown in Table 5, under the existing wind conditions in Shanghai and Shenzhen, the fatigue life of the double-sided semi-closed noise barrier

can exceed 50 years under all working conditions, thereby meeting the code requirement but in Beijing, the fatigue life of double-sided noise barrier exceeds 50 years when the train speed is less than 350 km/h, otherwise, it cannot reach 50 years. However, the fatigue life of the single-sided semi-closed noise barrier is less than 50 years under almost all working conditions, except the sections with low trains meeting ratio in Shanghai. Therefore, under the combined load of the natural wind and train aerodynamic impulse wind, the potential damage risk of the semi-closed noise barrier increases with the increase of service time. Therefore, the single-sided semi-closed noise barrier should be monitored regularly and reinforced in time to ensure its stability. Moreover, it is also an effective measure to prolong the fatigue life of the noise barrier by appropriately reducing the train speed and the trains meeting ratio in the noise barrier area.

5. Discussion

The semi-closed noise barrier is a common measurement to reduce the noise along the HSR, its fatigue safety performance directly affects the driving safety and engineering operation cost. Fatigue life prediction for noise barriers can guide the structural maintenance and reinforcement in practice, thus extending the service time and enhances the sustainability of noise barriers.

Previous studies on fatigue performance of noise barriers were mainly conducted through field experiments and monitoring the states of noise barrier components in some specific projects. However, from the study above, it can be found that the fatigue life of noise barriers is different in regions with different wind conditions. Even in the same region, under different train operation conditions, the fatigue life of noise barriers in each railway section is different. Therefore, there is little reference for extending the experimental research conclusions in a specific project to other projects. In this study, a theoretical calculation method for the fatigue life prediction of noise barriers was proposed through numerical simulation. According to the wind conditions and train operation conditions of the target railway section, the fatigue life of noise barriers can be predicted, which is more universal and sustainable. The fatigue life prediction for semi-closed noise barriers can prevent entirely replacing noise barrier structures, thereby effectively reducing the operation cost. Moreover, targeted reinforcement based on the actual state of the noise barrier under different operation conditions can also prevent the waste of materials, making the service process of the noise barriers more eco-friendly and realizing sustainable development.

In addition, in Kim's research [21], the digital twin-based noise barrier is a great monitoring system for the noise barriers, which can estimate the lifespan from the physical states of noise barrier components. However, this system cannot predict the fatigue life of noise barriers in each railway section before installment, so the reference it provides in the design stage is limited. The main reason that the digital twin-based noise barrier cannot be widely applied is that the manufacturing and installation costs are too high to be used in the whole noise barrier area. Our research can serve as a good reference for the engineering application of the digital twin-based noise barrier. Firstly, according to the wind conditions and train operation conditions in the target region, the noise barrier sections with high damage risk are calculated and forewarned through the fatigue life prediction method we proposed, such as the sections with high train speed and high trains meeting ratio. Then, the digital twin-based noise barrier can be applied only in these high-risk sections, which can greatly reduce the costs. The maintenance cycle period of the noise barrier in high-risk sections can be determined by real-time state monitoring of the noise barrier and its components, which increases the sustainability of noise barrier maintenance.

Based on the research results above, the following suggestions are put forward for prolonging the fatigue life of the semi-closed noise barrier in practical engineering:

(1) When the construction land and funds are sufficient, the double-sided semi-closed noise barrier should be adopted. The increased installation costs are worthy compared with the reduced maintenance costs and better train safety.

(2) The train speed should be appropriately limited when passing through the noise barrier area. Especially when the wind speed level exceeds 4, a train speed limitation in the noise barrier area can be considered.

(3) Appropriately reducing the train speed and the trains meeting ratio in the noise barrier area is an effective measure to prolong the fatigue life of the noise barrier.

(4) On the basis of life prediction for noise barriers, a digital twin-based noise barrier can be adopted in high-risk sections, and the structure should be regularly inspected and maintained.

This study provides theoretical support for the design stage of semi-closed noise barriers and is instructive for maintenance. However, there are a few limitations associated with the study. The influence of wind load on the noise barrier was analyzed in this study but was limited by theoretical development; the cumulative effects of humidity, temperature cycle, and initial defects of structural components on noise barrier performance were not under consideration. Considering multiple influencing factors, more accurate fatigue life prediction for noise barrier will be the focus in our future study to enhance sustainability.

6. Conclusions

In this paper, the CFD and FEM models of the semi-closed noise barrier were established, and the random natural wind and train aerodynamic impulse wind were simulated to study the influence of wind load on the noise barrier. Then, based on the rain flow counting method and Miner linear cumulative fatigue damage theory, a fatigue life prediction method for noise barriers was proposed. According to the wind conditions and train operating modes, the fatigue life of noise barriers in Beijing, Shanghai, and Shenzhen was calculated. Furthermore, some engineering suggestions for prolonging the fatigue life of noise barriers were put forward. From the results of the study, the following conclusions can be made:

(1) The natural wind pressure on the semi-closed noise barrier increases with the increase of the wind speed, and the growth rate increases continuously. (2) The aerodynamic impulse pressure on the semi-closed noise barrier increases with the increase of the train speed. The peak pressure on the double-sided noise barrier is higher than that on the single-sided one. Also, the aerodynamic impulse pressure caused by two trains meeting is higher than that caused by a single train running. (3) Compared with the single-sided semi-closed noise barrier, the double-sided noise barrier has better integrity, lower equivalent stress, and longer fatigue life. (4) Under different wind conditions and train operation conditions, the fatigue life of a noise barrier is different. Under natural wind load, the stronger the wind, the shorter the fatigue life of the semi-closed noise barrier; under aerodynamic impulse wind load, the fatigue life of the noise barrier decreases with the increase of the train speed and the trains meeting ratio. (5) Targeted maintenance of noise barriers in different fatigue states leads to less material needs and maintenance workload, which is more economical and eco-friendly. (6) It is beneficial to prolong the fatigue life and the sustainability of the noise barrier by appropriately reducing the train speed and train meeting ratio in the noise barrier area.

Author Contributions: Conceptualization, X.W. and Y.Z.; methodology, L.X.; software, Y.Z. and L.X.; validation, Y.Z.; formal analysis, Y.Z.; investigation, Y.H.; writing—original draft preparation, X.W. and Y.Z.; writing—review and editing, X.W. and Y.Z.; visualization, Y.H. All authors have read and agreed to the published version of the manuscript.

Funding: This research was funded by the Major Program of National Natural Science Foundation of China, grant number 51878672 and the Transportation Science and Technology Project of Hunan Province, grant number 201901.

Institutional Review Board Statement: Not applicable.

Informed Consent Statement: Not applicable.

Data Availability Statement: The data presented in this study are available on request from the corresponding author.

Conflicts of Interest: The authors declare no conflict of interest.

References

1. Mellet, C.; Létourneaux, F.; Poisson, F.; Talotte, C. High speed train noise emission: Latest investigation of the aerodynamic/rolling noise contribution. *J. Sound Vib.* **2005**, *293*, 535–546. [CrossRef]
2. Lauterbach, A.; Ehrenfried, K.; Loose, S.; Wagner, C. Microphone array wind tunnel measurements of reynolds number effects in high-Speed train aeroacoustic. *Int. J. Aeroacoust.* **2012**, *11*, 411–446. [CrossRef]
3. Ivanov, N.I.; Boiko, I.S.; Shashurin, A.E. The problem of high-speed railway noise prediction and reduction. *Procedia Eng.* **2017**, *189*, 539–546. [CrossRef]
4. Stepan, D.; Ionel, I.; Stefanescu, W. Noise control in railway vehicles. *J. Environ. Prot. Ecol.* **2012**, *13*, 561–570.
5. Guzas, D.; Tricys, V. Noise in European railway under modernization and its reduction. *J. Vibroeng.* **2010**, *12*, 649–656.
6. Karimi, M.; Younesian, D. Optimized T-Shape and Y-Shape inclined sound barriers for railway noise mitigation. *J. Low Freq. Noise Vib. Act. Control* **2014**, *33*, 357–370. [CrossRef]
7. Baulac, M.; Defrance, J.; Jean, P. Optimisation with genetic algorithm of the acoustic performance of T-shaped noise barriers with a reactive top surface. *Appl. Acoust.* **2006**, *69*, 332–342. [CrossRef]
8. Li, Q.T.; Duhamel, D.; Luo, Y.Y.; Yin, H. Analysing the acoustic performance of a nearly-enclosed noise barrier using scale model experiments and a 2.5-D BEM approach. *Appl. Acoust.* **2020**, *158*, 107079. [CrossRef]
9. Zhang, X.; Liu, R.; Cao, Z.Y.; Wang, X.Y. Acoustic performance of a semi-closed noise barrier installed on a high-speed railway bridge: Measurement and analysis considering actual service conditions. *Measurement* **2019**, *138*, 386–399. [CrossRef]
10. Li, X.Z.; Zhao, Q.C.; Zhang, X.; Yang, D.W. Test and analysis of noise reduction effect of semi-enclosed noise barrier on high-speed railway. *J. Southwest Jiaotong Univ.* **2018**, *53*, 661–669, 755.
11. Tokunaga, M.; Sogabe, M.; Santo, T.; Ono, K. Dynamic response evaluation of tall noise barrier on high speed railway structures. *J. Sound Vib.* **2016**, *366*, 293–308. [CrossRef]
12. Liu, Z.H.; Wang, Y.Q.; Wei, X.W. Adaptative study of closed and semi-closed noise barriers in a 3D ray tracing method. In Proceedings of the Environment and Transportation Engineering, Nanjing, China, 24–26 June 2011; pp. 7339–7342.
13. Zhou, Q.; Zhang, X.; Hao, C.X.; Li, X.; Li, X.Z.; Zheng, S.H. Field measurement and prediction model of acoustic performance of semi-closed noise barrier of high-speed railway. *J. Railw. Eng.* **2020**, *42*, 127–133.
14. He, J.J.; Xiang, H.X.; Ceng, M.; Li, Y.L.; Peng, D. Numerical simulation of pressure wave load of trains with totally enclosed noise barrier on high-speed railway bridges. *Vib. Shock.* **2020**, *39*, 175–182.
15. Luo, Y.K.; Zhang, X.; Li, X.Z. Vibration analysis of semi-enclosed noise barriers on bridges under wheel-rail dynamics. *Vib. Shock.* **2018**, *37*, 255–262.
16. Jing, Z.; Li, Q.L.; Li, X.Z. Train-induced fluctuating pressure and resultant dynamic response of semi-closed sound barriers. *Shock Vib.* **2020**, *2020*, 6901564.
17. Li, M.; Jiao, W.X.; Liu, W.X.Z.; Song, Y.J.; Chang, L.Q. A Method for peak seeking of BOTDR based on the incomplete brillouin spectrum. *IEEE Photonics J.* **2015**, *7*, 1–10. [CrossRef]
18. Di Mascio, P.; Loprencipe, G.; Moretti, L. Competition in rail transport: Methodology to evaluate economic impact of new trains on track. In Proceedings of the 3rd International Conference on Transportation Infrastructure ICTI2014–Sustainability, Eco-Efficiency and Conservation in Transportation Infrastructure Asset Management, Pisa, Italy, 28 April 2014; pp. 22–25.
19. Keller, T.; Riebel, F.; Till, V. GFRP posts for railway noise barriers—Experimental validation of load-carrying performance and durability. *Compos. Struct.* **2008**, *85*, 116–125. [CrossRef]
20. Yuan, S.; Xu, Y.R.; Wang, X.M.; Zhu, H.P. Experimental studies on column foot connections of novel fully enclosed noise barriers. *J. Constr. Steel Res.* **2020**, *172*, 106179.
21. Lachinger, S.; Reiterer, M.; Kari, H. Comparison of calculation methods for aerodynamic impact on noise barriers along high speed rail lines. In Proceedings of the 11th World Congress on Railway Research, Milan, Italy, 29–31 May 2016; pp. 1–7.
22. Kim, J.; Kim, S.A. Lifespan prediction technique for digital twin-based noise barrier tunnels. *Sustainability* **2020**, *12*, 2940. [CrossRef]
23. Wiesner, C.S.; Maddox, S.J.; Xu, W.; Webster, G.A.; Burdekin, F.M.; Andrews, R.M.; Harrison, J.D. Engineering critical analyses to BS 7910—The UK guide on methods for assessing the acceptability of flaws in metallic structures. *Int. J. Pres. Ves. Pip.* **2000**, *77*, 883–893. [CrossRef]
24. Lukács, J. Dimensions of lifetime management. *Mater. Sci. Forum* **2005**, *473–474*, 361–368. [CrossRef]
25. Hunt, J.; Wray, A.; Moin, P. Eddies, Stream, and Convergence Zones in Turbulent Flows. In *Studying Turbulence Using Numerical Simulation Databases, Proceeding of the Summer Program in Center for Turbulence Research, San Francisco, CA, USA, 1 December 1988*; Center for Turbulence Research: Stanford, CA, USA, 1988; pp. 193–208.
26. Kaimal, J.; Wyngaard, J.; Lzumi, Y.; Cote, O. Spectral characteristics of surface layer turbulence. *J. R. Meteorol. Soc.* **1972**, *98*, 563–589. [CrossRef]
27. Ministry of Transport of the People's Republic of China. *Wind-Resistant Design Specification for Highway Bridges JTG/T 3360-01-2018*; China Communications Publishing & Media Management CO., Ltd.: Beijing, China, 2018.

28. Davenport, A.G. The spectrum of horizontal gustiness near the ground in high winds. *Q. J. R. Meteorol. Soc.* **1961**, *87*, 194–211. [CrossRef]
29. Ma, S.H.; Ma, Y.J. Effects of maximum instantaneous wind velocity on the safety of high-speed train and its control. *J. Railw. Eng. Soc.* **2009**, *26*, 11–16.
30. Ministry of Housing and Urban-Rural Development of the People's Republic of China. *Load Code for the Design of Building Structures GB50009—2012*; China Architecture & Building Press: Beijing, China, 2012.
31. Li, X.B.; Yang, Z.; Zhang, J.Y. Aerodynamic properties of high-speed train in strong wind. *J. Traffic Transp. Eng.* **2009**, *9*, 66–73.
32. Scholz, M.; Buba, Z.; Boruttau, M. *Consulting Report: Noise Barrier for High Speed Railway*; Germany Planning Engineering Consulting + Services Ltd.: Beijing, China, 2007.
33. Miner, M.A. Cumulative damage in fatigue. *J. Appl. Mech.* **1945**, *67*, 51–56.
34. Ministry of Housing and Urban-Rural Development of the People's Republic of China. *Standard for Design of Steel Structures GB 50017—2017*; China Architecture & Building Press: Beijing, China, 2017.
35. China Railway Design Group Co., Ltd. *Installation Drawing of Inserted Metal Noise Barrier on High-Speed Railway Bridges for Train Speed of 250km/h and 350km/h TH2016(8323)*; China State Railway Group Co., Ltd.: Beijing, China, 2017.